

Considerable non-local electronic correlations in strongly doped Na_xCoO_2

Christoph Piefke,¹ Lewin Boehnke,¹ Antoine Georges,² and Frank Lechermann¹

¹*I. Institut für Theoretische Physik, Universität Hamburg, D-20355 Hamburg, Germany*

²*Centre de Physique Théorique, École Polytechnique, CNRS, 91128 Palaiseau Cedex, France*

The puzzling electronic correlation effects in the sodium cobaltate system are studied by means of the combination of density functional theory and the rotationally invariant slave boson (RISB) method in a cellular-cluster approach. Realistic non-local correlations are hence described in the short-range regime for finite Coulomb interactions on the underlying frustrated triangular lattice. A local Hubbard U is sufficient to model the gross in-plane magnetic behavior with doping x , namely antiferromagnetic correlations at intermediate doping and the onset of ferromagnetic order above $x > 3/4$ with a mixed phase for $0.62 < x < 3/4$. Important insight is thereby provided by the occupations of local cluster multiplets retrieved from the RISB framework. The extended modeling of the $x \geq 2/3$ doping regime with an additional inter-site Coulomb repulsion V on an experimentally verified effective kagomé lattice allows to account for relevant charge-ordering physics. Therewith a fluctuating charge-density-wave state with small quasiparticle weight and a maximum in-plane magnetic susceptibility may be identified at $x \sim 3/4$, just where the magnetic ordering sets in.

PACS numbers: 71.27.+a, 71.30.+h, 71.10.Fd, 75.30.Cr

I. INTRODUCTION

The investigation of frustrated spin systems plays a vital role in condensed matter physics due to its immediate importance for the understanding of competing interactions¹. However many realistic frustrated systems are insulating and may not be metalized via doping. Hence studying frustration effects within the metallic regime and possibly tuning interactions by additional doping can often only be realized in a pure model context. Nonetheless, there is growing awareness that such effects are also important in correlated metals². For instance it is believed by many researchers that for the recently discovered high-temperature superconducting iron pnictides³, spin and/or orbital frustration is a relevant feature^{4,5}.

Concerning the doping possibility of a strongly correlated metal with manifest geometrical frustrations, sodium cobaltate Na_xCoO_2 serves as an unique realistic test case. This system consists of stacked triangular CoO_2 layers, held together by Na ions inbetween. Nominally, the oxidation state of cobalt ranges between $\text{Co}^{4+}(3d^5)$ and $\text{Co}^{3+}(3d^6)$, depending on the doping x . Because of the strong (t_{2g}, e_g) crystal-field (CF) splitting a low-spin state is believed to be realized for the Co ion, where x controls the final filling of the rather localized t_{2g} manifold. Due to the additional trigonal t_{2g} -internal $a_{1g}-e'_g$ splitting, x thus formally mediates in a simplified view between a remaining half-filled a_{1g} orbital ($x=0$) and the band-insulating regime ($x=1$). In this respect however the trigonal CF splitting appears to be a crucial parameter. Calculations based on the local density approximation (LDA) yield a value $\Delta(a_{1g}-e'_g) \sim -0.1$ eV for $x=0.5$, decreasing in magnitude away from this doping level^{6,7}. Yet the measured Fermi surface (FS) shows only a single distinct hole-like hexagonal sheet, whereas LDA predicts additional e'_g hole pockets. Further investigations have underlined the subtleties associated with this CF splitting for the cobaltate system⁸⁻¹¹. Note that a

single hole-like FS sheet would transfer into a low-energy single-band modeling with a negative nearest-neighbor (NN) hopping t . Already on this level, an interesting interplay between the various degrees of freedom (spin, orbital and charge) is expected, where the geometrical frustration together with a large ratio U/W of the Hubbard U and the bandwidth W should result in a complex behavior with x .

Experimental investigations have indeed revealed a very rich phase diagram, incorporating various rather different many-body phenomena and phases. A superconducting dome ($T_c \sim 4.5$ K) appears close to $x=1/3$ when intercalation with H_2O is allowed for¹², while a metal-insulator transition (MIT) is found¹³ for $x=0.5$ below $T_{\text{MIT}} \sim 51$ K. Above $x=0.5$ a disproportionation of charge between the Co sites takes place^{14,15} and a regime of large thermopower is detected¹⁶ for $0.71 < x < 0.84$. In view of the possible frustration effects, the varying magnetic behavior is a central concern. For low doping in the range $x < 0.5$ an overall Pauli-like susceptibility is found¹³ with however hints for two-dimensional (2D) antiferromagnetic (AFM) correlations^{15,17,18}. Such AFM correlations are identified to increase towards $x=0$ for the structurally similar Li_xCoO_2 system¹⁹. Yet isolated CoO_2 , i.e., $x=0$, appears to be metallic, whereby the degree of electronic correlations is still a matter of debate^{19,20}. The case $x=0.5$ seems exceptional, with in-plane AFM order²¹ in the insulating regime. For $x > 0.5$ the system displays increasing magnetical response with a spin-fluctuation regime in the range $0.6 < x < 3/4$, including the evolution to Curie-Weiss behavior¹³ for $0.6 < x < 0.67$, and the eventual onset of in-plane ferromagnetic (FM) order^{15,22-30}. The magnetic structure in the doping range $3/4 < x < 0.9$ with ordering temperatures $T_N \sim 19-27$ K^{21-24,27} is of A-type, i.e., the FM CoO_2 layers are coupled antiferromagnetically.

The fact that not the low-doping regime with the nominal Co^{4+} ($S=1/2$) state (close to $x=0$) but the high-

doping region with the nominal Co^{3+} ($S=0$) state (close to $x=1$) is the magnetically active part in the phase diagram has motivated various theoretical efforts. Early LSDA computations^{31,32} predicted an itinerant FM solution for all doping levels between $0.3 < x < 0.7$, clearly in contradiction with experimental findings. In more recent calculations Johannes *et al.*³³ were able to show that an A -type AFM structure is slightly favored over the FM state for a simple approximant to the realistic cobaltate crystal structure at $x=2/3$. Generally the different ordered magnetic LSDA states are indeed rather close in energy³¹.

Aside from the already named indications, the relevance of correlation effects beyond LDA due to the partially filled $\text{Co}(3d)$ shell has been motivated by several experiments, e.g., from optics³⁴, photoemission³⁵⁻³⁸ and transport¹³ measurements. In view of the cobaltate physics, Merino *et al.*³⁹ discussed in detail the electron-doped single-band Hubbard model with NN hopping on the triangular lattice within single-site dynamical mean-field theory (DMFT). There it was concluded that for $t > 0$ the paramagnetic (PM) Curie-Weiss metallic phase has an instability towards FM order for large enough U/W . However such a transition is missing for the case $t < 0$, where moreover the PM metallic phase displays Pauli-like magnetic response. In Na_xCoO_2 the dominant NN hopping appears indeed to be negative, but relevant higher hopping amplitudes (at least to 3rd order) are necessary to bring the tight-binding (TB) modeling in good accordance with the LDA dispersion^{40,41}. These higher contributions introduce a flatness to the low-energy band, giving rise to substantial additional structure in the density of states (DOS) compared to the NN-TB DOS^{6,42}. This allows for a more interesting magnetic behavior with electron doping in contrast to the simplified NN-TB ($t < 0$) model. In fact the study of Korshunov *et al.*⁴³ based on the combination of the realistic three-band (a_{1g} , e'_g) dispersion with a Hubbard on-site interaction resulted in ($\mathbf{q}=0$)-peaks in the magnetic susceptibility at around $x_p \sim 0.56$ ($U=0$ eV), $x_p \sim 0.6$ (infinite- U Gutzwiller) and $x_p \sim 0.68$ (infinite- U Hubbard I). Gao *et al.*⁴⁴ obtained in similar calculations using a single-band third NN-TB model also within infinite- U Gutzwiller a corresponding value $x_p \sim 0.67$. In a charge-selfconsistent doping-dependent LDA+Gutzwiller treatment with three correlated (a_{1g} , e'_g) orbitals the A -type AFM order was found to be stable for $x > 0.6$ ($U=3$ eV) and $x > 0.5$ ($U=5$ eV) by Wang *et al.*⁹, but with additional findings of FM order for $x < 0.3$. Note that all these correlated studies neglect non-local effects of strong correlation, i.e., the self-energy is taken to be local and, importantly, a single correlated Co site in the respective planar part of the unit cell is assumed. Moreover the doping dependence of the system is simulated via simple band filling or the virtual crystal approximation (VCA)⁴⁵. In a single-site DMFT study by Marianetti and Kotliar the importance of the Na positions for the strong correlation effects was actually demonstrated⁴⁶.

Interestingly, another cobaltate modeling⁴⁷ applying the t - J model with only NN-TB ($t < 0$) hopping (and simple doping description), solved via exact diagonalization on clusters as big as 18 sites (with periodic boundary conditions) yield Curie-Weiss behavior for $x < 3/4$ in contrast to the single-site DMFT Hubbard-model studies³⁹. In addition recent experimental findings⁴⁸ show evidence for a kagomé-lattice imprint due to intricate Na ordering at $x=2/3$. These are only two hints towards the need for a reinforced description of non-local correlations in the cobaltate theory, strengthening also the original aspect of the relevance of the geometric frustrations. Both advanced aspects, i.e., strong non-local correlations and a more elaborate doping dependence within a realistic framework were combined in Ref. 49. There the realistic LDA dispersions for a three-site Na_xCoO_2 in-plane cluster were supplemented with a finite Hubbard interaction in a cellular-cluster application of the rotationally invariant slave boson (RISB) method^{50,51}. Note that there in the construction of the doping-dependent LDA Hamiltonian the respective crystal fields within the triangular cluster (modified by close-by Na ions) were not site-averaged as in the VCA approaches.

In the present work we want to extend the considerations of Ref. 49 by a detailed investigation of the cluster multiplets in the realistic three-site cluster approach to Na_xCoO_2 . Galanakis *et al.*⁵² performed a similar study for the doped Hubbard model on the triangular lattice using the non-crossing approximation (NCA) to cellular DMFT, but without incorporating realistic band dispersions and without elucidating magnetism.

II. THEORETICAL APPROACH

A. Realistic modeling

We describe the sodium cobaltate system from a strongly correlated perspective within a realistic framework. This however does not presume that Na_xCoO_2 may be pictured as a doped Mott insulator, a viewpoint often taken for the physics of high temperature superconductivity⁵³. Instead here the interplay of correlation and frustration effects in an itinerant Fermi-liquid(-like) state with the important proximity to the band-insulating ($x=1$) state appear to be the main characteristics. The Fermi-liquid character renders the LDA description as a reasonable initial starting point. Furthermore the chemical aspects due to the intriguing ordering behavior of the sodium ions across the x - T phase diagram brings additional importance to a careful investigation of the realistic electronic structure with doping. Still because of the narrow bandwidth of the low-energy sector, even moderate values of the local Coulomb repulsion on a given Co site puts one in the regime $U/W \geq 1$. Thus neglecting this fact may not be adequate on the way to a complete theory of this materials system.

It is aimed for a non-local approach in order to al-

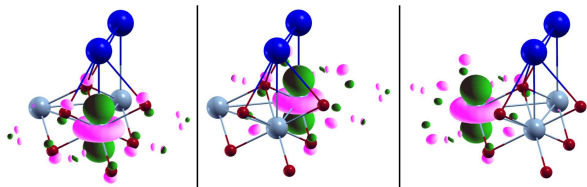


FIG. 1: (Color online) a_{1g} -like Wannier-like functions in the Na_xCoO_2 super cell for $x=2/3$. Large blue (dark) balls denote Na ions, light blue (light gray) balls Co ions, small red (gray) balls mark O ions.

low for inter-site self-energy effects on the triangular lattice. To this, as a first approximation, the minimal three-site cluster with on-site Hubbard interactions is identified as the canonical model. For the lattice description a cellular-cluster methodology shall serve as method of choice to combine the NN inter-site correlations with the overall itinerant behavior. This extended approach beyond the single-site description is supplemented with realistic Kohn-Sham (KS) dispersions from LDA in a Wannier-like basis utilizing the maximally-localized technique^{54,55}. The underlying band-structure calculations are performed using a mixed-basis pseudopotential implementation⁵⁶. This method⁵⁷ utilizes norm-conserving pseudopotentials with a combined basis set of plane waves and non-overlapping localized functions.

In the construction of the realistic model the question concerning the correlated subspace, i.e., the nature and number of included correlated orbitals, arises. In principle the full $(a_{1g}, e'_g) t_{2g}$ manifold appears as the suitable minimal choice. Yet treating a metallic state by a three-site cluster with altogether nine interacting orbitals and reduced symmetries in a large doping range is numerically very heavy for any well-suited many-body technique. But note that the experimental FS studies reveal only a single a_{1g} -like band at the Fermi level and also the basic LDA studies predict the e'_g -like bands close to complete filling. In addition, in this work we are mainly interested in the magnetic behavior at larger doping where in any case these e'_g -like bands sink even deeper in energy. Hence we reduce the correlated subspace to three effective a_{1g} orbitals per Co cluster, to be determined by the Wannier-like construction and therefore including hybridization effects with the remaining orbitals. This approach seems also suitable from a local-correlation point of view since the (nearly) filled e'_g orbitals are in a singlet state (low-spin Co) and thus do not give rise to additional spin scattering. In other words, double-exchange processes are expected to be irrelevant. At small doping however the inclusion of the e'_g orbitals seems necessary because of an apparent increased relevance of the multi-orbital character. For the interesting magnetic properties at larger doping one expects the non-local correlations to dominate any intrasite multi-orbital correlations in this specific filling scenario.

A meaningful and numerically efficient characteriza-

tion of the complex doping behavior may be build on LDA calculations at selected doping levels. A supercell involving the NN Co triangle of a given CoO_2 layer serves as the base structure. By decorating this triangle with Na ions *above* the Co sites, i.e., usually called Na(1) position (see Fig. 1), we may represent the dopings $x=\{0, 1/3, 2/3, 1\}$. Note that in this simplified ansatz no sodium ions above/below oxygen positions, i.e., Na(2) positions, are considered. Albeit this limits the comparability to the true structures^{48,58,59} it allows for a discrimination of the Co sites with x and shall be sufficient for the overall behavior with doping. In addition we project from the start the obtained complete KS Wannier Hamiltonian to the 2D sector and treat only the in-plane dispersion within a given layer. Finally the doping-dependent 3×3 cluster band Hamiltonian is constructed through linear interpolation:

$$\mathbf{H}^{\text{KS}}(\mathbf{K}, x) = x\mathbf{H}_{x_a}^{\text{KS}}(\mathbf{K}) + (1-x)\mathbf{H}_{x_b}^{\text{KS}}(\mathbf{K}) \quad , \quad (1)$$

where x_a, x_b are the neighboring LDA-treated dopings and \mathbf{K} denotes the wave vector in the supercell formalism. Note that while VCA averages in *real* space, this kind of interpolation takes place in *reciprocal* space. Thereby the local differences between the Co sites remain vital throughout the doping scan. Note that the 2D-only approach is generalized to the full 3D case within the effective-kagomé-lattice modeling discussed in section V.

The complete many-body Hamiltonian for a given x to be solved within the cellular-cluster approach then reads as follows

$$H = \sum_{\mathbf{K}ij\sigma} \varepsilon_{\mathbf{K}ij} d_{\mathbf{K}i\sigma}^\dagger d_{\mathbf{K}j\sigma} + \sum_{\alpha} H_{\alpha} \quad , \quad (2)$$

where i, j are sites within the triangular cluster α , σ is the spin index and $d^{(\dagger)}$ is the electron annihilation (creation) operator. The local cluster Hamiltonian H_{α} shall consist of an quadratic on-site part, the local Hubbard U interaction term and possibly a NN inter-site Coulomb interaction term with amplitude V , i.e.,

$$H_{\alpha} = \sum_{ij\sigma} \varepsilon_{\alpha ij} d_{i\sigma}^\dagger d_{j\sigma} + U \sum_i n_{i\uparrow} n_{i\downarrow} + \frac{V}{4} \sum_{i \neq j, \sigma \sigma'} n_{i\sigma} n_{j\sigma'} \quad , \quad (3)$$

with $n_{i\sigma} = d_{i\sigma}^\dagger d_{i\sigma}$. To include the Coulomb coupling between NN clusters a mean-field (MF) decoupling of the inter-cluster interactions is performed, resulting in an embedding, which reads (dropping here the spin indices for convenience):

$$\sum_{i \neq j} n_i n_j \approx \sum_{i \neq j} (n_i \langle n_j \rangle + n_j \langle n_i \rangle - \langle n_i \rangle \langle n_j \rangle) \approx \sum_{i \neq j} n_i \langle n_j \rangle \quad , \quad (4)$$

where i is a site on the examined cluster and j is a site on the NN cluster. In the last step leading to eq. (4) it is assumed that the average value for n_j may be inserted. We neglect non-density-density terms in this MF

decoupling⁶⁰ since their effect should be minor. Hence the modified version of eq. (3) reads

$$H_\alpha = \sum_{ij\sigma} \varepsilon_{\alpha ij} d_{i\sigma}^\dagger d_{j\sigma} + U \sum_i n_{i\uparrow} n_{i\downarrow} + \frac{V}{4} \sum_{i \neq j, \sigma\sigma'} n_{i\sigma} \left(n_{j\sigma'} + \frac{1}{2} \langle n_{j\sigma'} \rangle \right) . \quad (5)$$

The factor $1/2$ in the MF term is needed to avoid the double counting of the inter-cluster Coulomb interaction when summing over α in eq. (2). In the actual calculation the values $\langle n_{j\sigma'} \rangle$ are initially set and then determined self-consistently via an outer loop to the RISB scheme. In a PM homogeneous case, the MF $\langle n_{j\sigma'} \rangle$ is independent of j and σ' and hence the contribution of that term corresponds to a mere chemical-potential shift. The justification of an (extended)-Hubbard-type Hamiltonian for sodium cobaltate may not straightforwardly be verified, because additional interaction terms could arise in a minimal model. However we believe this approach to be reliable for most of the key physics in cobaltates. Explicit exchange terms due the fact that we integrated out the oxygen states are expected to be small in size and are very difficult to compute for metals in a rigorous manner³³.

The dispersions are provided by the KS Hamiltonian of eq. (1) (spanned on N_K points in reciprocal space) in the following way:

$$\varepsilon_{\mathbf{K}ij} = H_{ij}^{\text{KS}}(\mathbf{K}, x) - \frac{1}{N_K} \sum_{\mathbf{K}} H_{ij}^{\text{KS}}(\mathbf{K}, x) , \quad (6)$$

$$\varepsilon_{\alpha ij} = \frac{1}{N_K} \sum_{\mathbf{K}} H_{ij}^{\text{KS}}(\mathbf{K}, x) . \quad (7)$$

Thus the dispersive part carries no local terms, all of those are transferred into H_α . In the solution of the problem one has to be aware of the breaking of translational invariance in the cellular cluster scheme (for reviews of cluster approaches to strongly correlated systems see e.g. Ref. [61–63]). Since no detailed K-dependent properties are discussed, no periodization of the resulting cluster self-energy is performed in the present work.

B. RISB method

The full Hamiltonian from eq. (2) is solved employing the rotationally invariant slave boson (RISB) formalism^{50,51} in the saddle-point approximation. Within RISB the electron operator $d_{i\sigma}$ is represented as $\underline{d}_{i\sigma} = \hat{R}[\phi]_{ij}^{\sigma\sigma'} f_{j\sigma'}$, where R is a non-diagonal transformation operator that relates the physical operator to the quasiparticle (QP) operator $f_{i\sigma}$. The transformation \hat{R} is written in terms of the slave bosons $\{\phi_{An}\}$. In this generalized slave-boson theory ϕ carries two indices, namely A for the physical-electron state and n for the QP Fock state. It follows that the kinetic K -dependent part of eq.

(2) is expressed via the QP operators with renormalized dispersions. The operator character of the local cluster part is described solely via the slave bosons⁵¹. In order to facilitate this operator decomposition into an QP part and the interacting part carried by the slave bosons, two constraints have to be enforced. They shall normalize the total boson weight to unity and ensure that the QP and boson contents match at every site, respectively:

$$\sum_{An} \phi_{An}^\dagger \phi_{An} = 1 , \quad (8)$$

$$\sum_{Ann'} \phi_{An'}^\dagger \phi_{An} \langle n | f_{i\sigma}^\dagger f_{j\sigma'} | n' \rangle = f_{i\sigma}^\dagger f_{j\sigma'} . \quad (9)$$

This selection of the physical states is imposed through a set of Lagrange multipliers $\{\lambda\}$. In the mean-field version at saddle-point these constraints hold on average, with the bosons condensed to c numbers. The solved saddle-point equations for $\{\phi\}, \{\lambda\}$ yield a free-energy F of the interacting electron system that may be used to investigate phase stabilities. Of course, this free energy shall not be confused with the total free energy of the system that also incorporates further terms, e.g., the nuclei contributions. However already therefrom, many important insights in the possible instabilities can be retrieved. Note that the K-point integration with a smearing method (Fermi, Gaussian) introduces a small effective temperature into the system, which however may not easlily be interpreted as a true physical temperature due to the fully-condensed boson treatment in this simplest mean-field approach.

The RISB physical self-energy of the d electrons at saddle-point is given by⁵¹

$$\Sigma_d(\omega) = \omega (1 - \mathbf{Z}^{-1}) + [\mathbf{R}^\dagger]^{-1} \mathbf{\Lambda} \mathbf{R}^{-1} - \varepsilon^{(0)} , \quad (10)$$

where $\mathbf{Z} = \mathbf{R} \mathbf{R}^\dagger$ is the QP-weight matrix and $\mathbf{\Lambda}$ is the lagrange-multiplier matrix. The quantity $\varepsilon^{(0)}$ is identical to the one-body term in the local Hamiltonian and hence in the present case its elements are given by eq. (7). Thus Σ_d contains only a term linear in frequency and a static part. Though more approximative than involved methods like, e.g., quantum Monte-Carlo, which may handle the full frequency dependence, this is sufficient to describe the QP nature at low-energy. It also gives an idea of the effect of local excitations within a static self-energy. In this regard, the slave-boson amplitudes yield direct access to the occupation of local multiplets in the metallic state. The RISB mean-field approach is moreover rather efficient with very reliable qualitative (and often even good quantitative) results in most cases. Note that though a lattice implementation of the this method is used here, the technique may equally well be utilized as an impurity solver for single-site DMFT⁶⁴. Due to the inherent local nature at saddle-point, this specific DMFT impurity solution is then identical to the direct lattice-calculation result.

In the present case the formalism is employed within a cellular-cluster context, i.e., the off-diagonal components

of the self-energy $\Sigma_d(\omega)$ describe inter-site correlation effects between the Co atoms in the triangular cluster. To obtain an intuitive interpretation for the slave-boson amplitudes, we rotate both the cluster- (A) and the QP- (n) index of ϕ_{An} into the eigenbasis Γ of the isolated cluster problem. The transformation matrix $\mathcal{U}(\Gamma)$ is obtained via simultaneous diagonalization of the commuting set of operators $\{H_\alpha, S^2, S_z, N\}$, where S is the total cluster spin operator, S_z its z -component and N the particle-number operator. Since H_α is a real, symmetric matrix, one ends up with a representation

$$\phi_{\Gamma\Gamma'} = \mathcal{U}_{\Gamma A}^\dagger \phi_{An} \mathcal{U}_{n\Gamma'} \quad (11)$$

in which the slave bosons $\phi_{\Gamma\Gamma'}$ are directly tailored to the multiplet structure of the local cluster α . Note that the given set of quantum numbers is still not sufficient to classify the cluster eigenstates completely. In order to simplify the presentation we limit however the discussion to this definition of the Γ basis, which is ample for the physics. In the following, a specific multiplet will be denoted $\Gamma_{p,n}^m$, where p describes the particle sector, n the energy level therein (starting with $n=0$ for the respective ground state) and m marks the spin state, i.e., singlet 's', doublet 'd', triplet 't' and quartet 'q'. Where quantum numbers are stated for a given multiplet, we follow standard Dirac notation $|E_{p,n}, S, S_z\rangle$ with E the multiplet energy, and S, S_z total spin and z -component respectively.

III. NN-TB MODEL ON THE TRIANGULAR LATTICE WITH LOCAL COULOMB INTERACTION

To give an introduction to our approach and to touch base with other recent work for the Hubbard model on the triangular lattice, we review here results of an NN-TB model with $t>0$. Hence V is put to zero in this section. This model considerations shall set the stage for a subsequent discussion of a more realistic model of Na_xCoO_2 with higher hopping terms and, importantly, a NN hopping $t<0$. We first investigate the isolated triangular cluster to understand the structure of the multiplet states and then relate these findings to the physics of the itinerant system.

A. Cluster states in the local limit

A detailed study of the Hubbard model on the triangular cluster, comparing the cases $t\leq 0$, has been presented in Ref. 39. There it was shown that the tendency towards ferromagnetism is indeed stronger for $t>0$ already in the local quantum-chemical problem. Here we only sketch the $t>0$ case and discuss the $t<0$ one in line with the realistic sodium cobaltate model in section IV.

Lets start with the relevant multiplet states on the non-interacting triangle within the different particle sec-

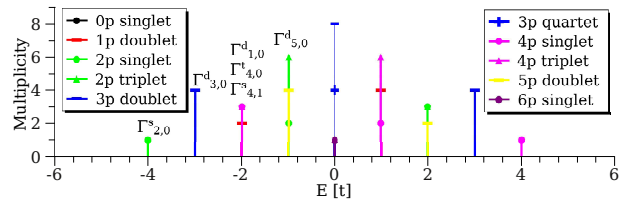


FIG. 2: (Color online) Triangular cluster spectrum of H_α for $U=0t$ and $t>0$. The height of each peak shows the respective multiplicity.

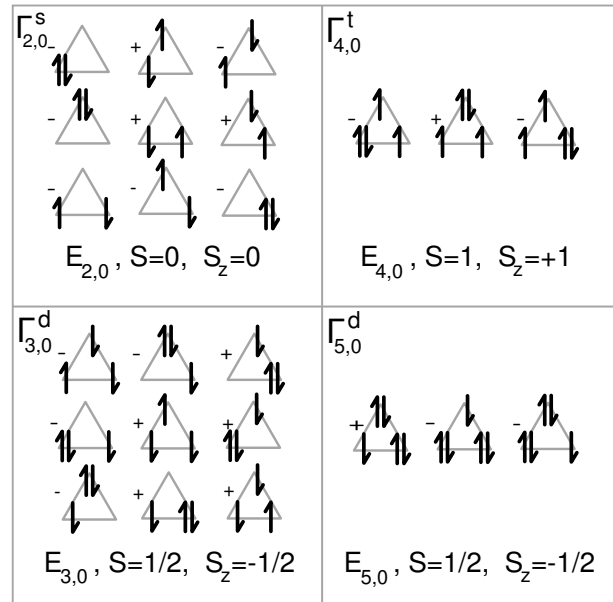


FIG. 3: Relevant cluster multiplets for the non-interacting TB model. The multiplets are shown as a superposition of Fock states. For pictorial simplicity, numerical factors are suppressed. Because the factors depend on U and x , the Fock states are sorted after the absolute value of the factors descending from left to right and top to bottom.

tors, obtained from a simultaneous exact diagonalization of $\{H_\alpha, S^2, S_z, N\}$. Note that in the present context H_α corresponds to eq. (3) with $\varepsilon_{\alpha ij} = -t(1 - \delta_{ij})$. Figure 2 displays the energy spectrum of the triangle in the non-interacting case, the decomposition of the corresponding eigenvectors into Fock states is shown in Fig. 3 for some relevant multiplets. For pictorial simplicity only the Fock states participating in a given multiplet are discussed, whereas the respective expansion coefficients are not shown, but of course are taken care of exactly within the calculations. In order to give an idea about the relative size of these coefficients, the pictorial expansion terms in Fig. 3 (and in the similar following figures) are ordered by the decreasing absolute value of the expansion coefficients.

The triangle spectrum of the NN-TB model displays a high degree of symmetry around zero energy in the non-interacting case. The lowest state in energy is a two-particle singlet, the highest state is given by a four-particle singlet. The isolated triangle with NN hopping

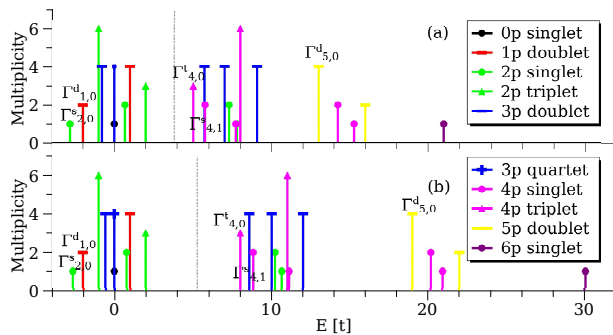


FIG. 4: (Color online) Triangular cluster spectrum of H_α for (a) $U=7t$ and (b) $U=10t$. Note the level crossing: a four-particle sector singlet passes a two-particle sector singlet and a four-particle sector triplet at $E \approx 10t$ for $U=7t$. No other level-crossings were observed for $t > 0$. The Fermi energy for the half-filled case of the itinerant problem is denoted by a dashed grey line for comparison.

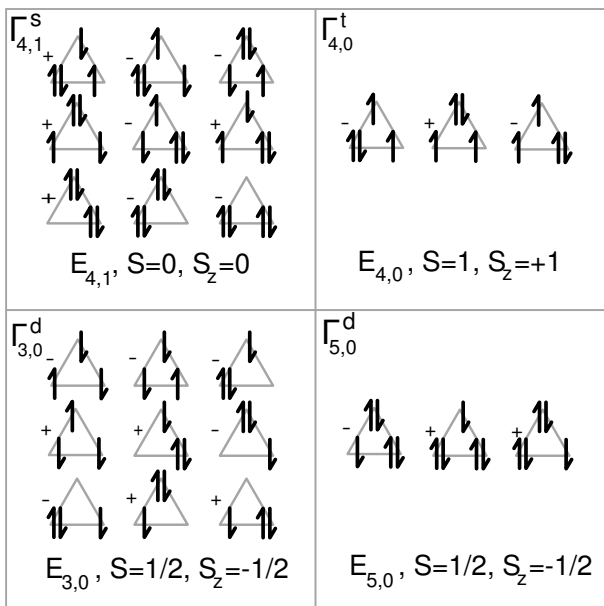


FIG. 5: Relevant cluster multiplets for the interacting TB model.

and $U=0t$ is anti-symmetric under exchange of particles and holes, two doublets from the three-particle sector show up at $E=\pm 3t$. The overall ground state is followed by the three-particle doublets, one-particle doublets and degenerated four-particle singlets and triplets at $E=-2t$. As pointed out in Ref. 39, the three different spin-orientations of the triplet in the four-particle sector are degenerated and the S_z state may be changed by spin flips without energy cost. The resulting high susceptibility for spin polarization in that particle sector is lost for the case $t < 0$. Figure 3 shows that for $t > 0$ the structure of the ground state in the four-particle sector is rather simple (but becomes more complex in the $t < 0$ case³⁹). The simplicity of the dominant doublet $\Gamma_{5,0}^d$ in the five-particle sector is due to the distribution of a single non-local hole, while the three-particle doublet $\Gamma_{3,0}^d$

as well as the two-particle singlet $\Gamma_{2,0}^s$ display a more complex decomposition into Fock states.

For $t > 0$ the electrons on the triangle can lower their energy via hopping. The multiplet $\Gamma_{2,0}^s$ contains nine Fock states and each electron in those states has two options of hopping, collecting one $-|t|$ every time. From a chemical point of view, a bonding state can always be formed. In the case of the three-particle ground state $\Gamma_{3,0}^d$, the unpaired electron enters an anti-bonding configuration, thus leading to a higher state energy.

Figure 4 shows the triangular cluster spectrum in the interacting regime for $U=7t$ and $U=10t$, the relevant multiplets in Fock-space decomposition are shown in Fig. 5. For the investigated U values, the two-particle singlet remains the overall ground state, because it only has to pay the U penalty for double occupation three times out of nine. It is energetically followed by the one-particle doublet which does not gain that much energy from hopping processes because of the single-electron occupation. But it now benefits from being free of U contributions. Hence with increasing U the overall ground state will eventually evolve towards this one-particle state via a “local Mott transition”. Note that the two-particle triplets are also not affected by U because they are also free of double occupations. The three-particle doublet which was following $\Gamma_{2,0}^s$ for $U=0$ eV, now has to pay the Coulomb penalty six times out of nine. On the other hand the three-particle doublets that show the high degree of multiplicity for the non-interacting case at zero energy split up for finite U . It is also interesting to remark that there is a swap in energy eigenvalues at $U \approx 9t$, i.e., the energy of a four-particle singlet increases faster in energy than the other states in this sector. Besides this one, no further level-crossings were observed with varying U . Again because of the lack of particle-hole symmetry, the two-particle sector is favored compared to the four-particle sector even at half filling. Note also that the four-particle triplet is lower in energy than the four-particle singlets. Thus in the atomic limit the triangle is still easy to polarize even for $U > 0$. This holds for the case of three-, four- or five-particle filling, since all energetically favorable states from these particle-sectors show a high degree of multiplicity and have a free spin. While for moderate U the overall ground state $\Gamma_{2,0}^s$ displays a very complex structure it has no free spin, compared to $\Gamma_{3,0}^d$.

B. Lattice modeling

In the cellular framework the infinite lattice is build up by finite clusters, here for the triangular case given by the minimal triangle (see Fig. 6). Since we are interested in the canonical 2D lattice, the inter-cluster hopping is identical to the intra-cluster one, i.e., the dispersive model is described by a NN-TB parametrization. In the non-interacting (Fermi gas) case the cellular formalism coincides with the standard single-site description,

where the bandwidth amounts to $W=9t$. Because of the absence of particle-hole symmetry the density of states (DOS) for smaller filling is strikingly different from the one at larger filling (cf. Fig. 6). A van-Hove singularity is located at $\varepsilon=\varepsilon_{\max}-t$ (ε_{\max} being the maximum single-particle energy for the single band), while such a singularity is missing at negative single-particle energies ε . Note that hence importantly the chemical potential for the half-filled case is *not* placed in the middle of the band.

For small Hubbard U the interacting model describes a Fermi liquid. We concentrate in the discussion on the paramagnetic regime of the half-filled as well as the electron-doped case. The resulting QP weight Z and inter-site spin correlation $\langle \mathbf{S}_i \cdot \mathbf{S}_j \rangle$ on the triangular cluster with increasing U at half filling are shown in Fig. 7(a,b). It is seen that the diagonal (onsite) QP weight Z_i decreases as U grows, until a first-order Mott transition is reached at $U_{c2} \approx 12.2t = 1.36W$. The off-diagonal (inter-site) elements Z_{ij} show opposite behaviour and increase towards U_{c2} , but are much smaller compared to Z_i . The literature on the critical U for the Hubbard model on the triangular lattice, without invoking magnetic order, is rather large. The present critical U is in the same range as values from exact diagonalization of a finite cluster⁶⁵ ($\sim 12.1t$) and cellular DMFT⁶⁶ ($\sim 10.5t$). Figure 7b shows that due to the dominant superexchange process at half filling the value for $\langle \mathbf{S}_i \cdot \mathbf{S}_j \rangle$ is always of AFM character, with a diverging slope at U_c .

Based on the local-cluster-limit study, the occupation of the extracted multiplets may now also be investigated in the itinerant problem. This allows for a discussion of the correlated metallic state for different Hubbard U and finite doping x from a finite-cluster real-space viewpoint. In this respect it may be observed in Fig. 8 that the cluster multiplet occupations are a valuable source of information. When discussing the condensed slave-boson amplitudes $\phi_{\Gamma\Gamma'}$ in that basis, we focus in the following on the first index Γ and sum over the second Γ' (of course, the full structure was used within the calculations). Note that the cluster dispersion on the lattice leads in the present case to (weakly) nondiagonal $\phi_{\Gamma\Gamma'}$ matrices. For small U , the non-degenerate two-particle

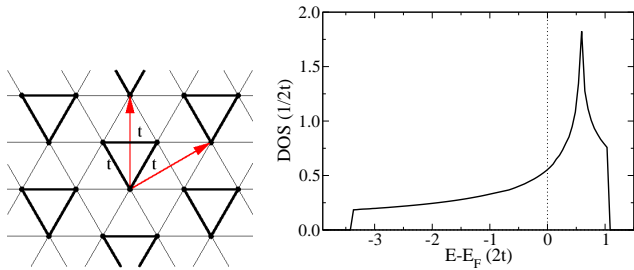


FIG. 6: (Color online) 3-site cellular cluster approach to the Hubbard model on the isotropic triangular lattice for NN hopping t . Left: lattice tiling, right: density of states with the Fermi energy E_F chosen for half filling.

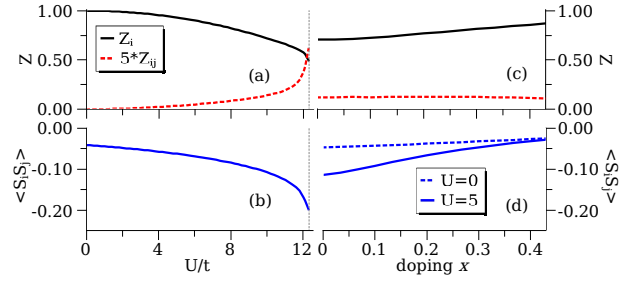


FIG. 7: (Color online) Observables for the NN-TB Hubbard model. U dependencies for (a) quasiparticle weight and (b) NN $\langle S_i S_j \rangle$ correlation functions at half filling. (c,d) same observables, but behavior with doping.

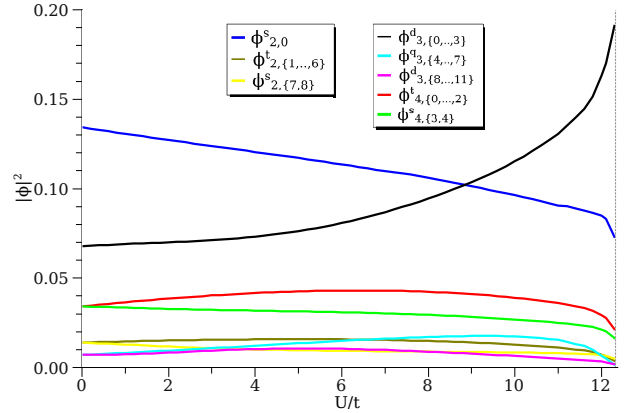


FIG. 8: (Color online) Relevant slave-boson amplitudes ϕ squared with increasing U for the cluster NN-TB model. The amplitudes are labeled with a single $\Gamma_{p,n}^m$ index (see text). The notation $\{i, \dots, j\}$ implies that the amplitudes for all states from i to j are of equal weight.

singlet $\Gamma_{2,0}^s$ has the highest occupation at half filling. However note that because of degeneracies the occupation of several other multiplets is identical, also allowing in principle for increased fluctuations among them. Thus the total occupation within such a class of multiplets, i.e., $\{\Gamma_{4,0}^t, \dots, \Gamma_{4,2}^t\}$ may be even higher. When normalized to single-multiplet occupations, the three-particle doublet states $|E_{3,0}^{d, 1/2, \pm 1/2}\rangle$ dominate for $U \gtrsim 9t$. Close to the Mott transition the paramagnetic system can be found nearly exclusively fluctuating between those two doublet states.

Figure 9 displays the slave-boson amplitudes with electron doping x up to an investigated regime of $x=0.425$ in the non-interacting case and at fixed $U=10t < U_c$. There the $U=0t$ case shows a simple crossover from the dominant $\Gamma_{2,0}^s$ at half filling to the six-particle singlet $\Gamma_{6,0}^s$ at larger filling (with statistical occupation of the remaining particle sectors). On the other hand for large U the four-particle triplet $\Gamma_{4,\{0,\dots,2\}}^t$ becomes strongest above $x \sim 0.2$. Note that the maximum of $|\phi_{4,\{0,\dots,2\}}^t|^2$ is reached around $x=1/3$ which is in the very same range as the onset of ferromagnetism in single-site DMFT for the given U value³⁹. The simple Stoner criterion is known

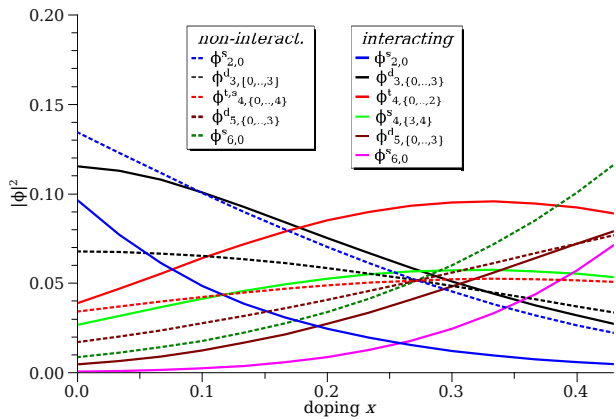


FIG. 9: (Color online) Doping-dependent slave-boson amplitudes in the NN-TB model for $U=0t$ and $U=10t$.

to fail in this context³⁹, e.g. for $x \sim 1/3$ the critical U_c^{FM} for ferromagnetism on the triangular lattice should be around $4t$. Thus the cluster viewpoint provided by the multiplet occupations in the RISB formalism, incorporating both, band dispersions and exchange mechanisms beyond Hartree-Fock, may serve as a good estimate for the magnetic ordering tendencies on the lattice. In this respect it is obvious that the large weight of the four-particle triplet renders the system rather susceptible to ferromagnetism by aligning the net spin of each basic triangle on the lattice. The dominance of the $\Gamma_{4,\{0,\dots,2\}}^t$ state around $x \sim 1/3$ is also in accordance with the recent findings of Galanakis *et al.*⁵² in their cellular-DMFT study using an NCA impurity solver.

IV. STRONGLY DOPED SODIUM COBALTATE WITH LOCAL COULOMB INTERACTION

This section deals with a realistic study of Na_xCoO_2 over a rather wide doping range based on projected LDA dispersions and explicit local on-site Coulomb interactions. Thus as in the previous section, $V=0$ eV holds here. We will show that such local Hubbard interactions within a cluster (or multi-site) modeling are sufficient to deliver a good description of the in-plane magnetic behavior with doping. Coming from lower x , the PM phase with AFM character as well as the onset of FM order at $x \sim 3/4$ results from this approach. A PM-FM mixed phase inbetween these regimes in the area $0.62 < x < 3/4$ is obtained, signaling a first-order scenario for this transition and the relevance of disorder/segregation effects for a deeper understanding of sodium cobaltate at large x .

As described in section II A, the realistic modeling of Na_xCoO_2 is based on the construction of an effective a_{1g} minimal cluster model. It is derived from the LDA description of chosen reference configurations (serving as simple approximants to the more complex true structures) for the dopings $x=\{0, 1/3, 2/3, 1\}$. The Wannier-like Hamiltonians are projected onto an effective single

x	$\Delta\varepsilon_{\text{Na}}$	t	t_2	t_3	t_4	t_{\perp}
0	0	-211	37	33	-6	24
1/3	-36	-173	34	30	-5	10
2/3	-48	-134	28	24	-4	15
1	0	-107	20	19	-2	20

TABLE I: Average hopping integrals for the Na_xCoO_2 cluster modeling from the effective a_{1g} Wannier-like construction shown here up to fourth-nearest neighbor (cf. Fig 6). The on-site level difference $\Delta\varepsilon_{\text{Na}}$ denotes the Na-induced level lowering for Co sites with sodium on top. Note that in the actual calculations the full 2D hopping matrices, i.e., not averaged and not restricted to 4th NN, were employed. The inter-layer hopping t_{\perp} is shown for comparison and did not enter the RISB calculations discussed in this section. Values are given in meV.

layer, i.e., the RISB method is faced with a 2D dispersion. The averaged in-plane hopping amplitudes obtained from the respective Wannier-like construction are given in Tab. I. Compared to the pure model case in the last sections, the NN t is now negative. It is moreover evident that the absolute value of t decreases with increasing doping x , in the end losing about half its magnitude towards $x=1$. This fact already points to a diminishing superexchange process at larger x . The higher hopping integrals (shown here up to fourth-NN) decay quickly with distance and also decrease in magnitude with doping. Note that the on-site levels are lowered by putting sodium on top. This can easily be understood by the attractive Coulomb potential introduced by the Na^+ ions. In Tab. I the NN inter-layer hoppings t_{\perp} are also provided. They show non-monotonic behavior with x and an expected slight increase of the three-dimensional (3D) character through the ratio t_{\perp}/t with doping. However these and higher inter-layer hoppings are not taken into account in the lattice studies presented in section IV B.

A. Cluster states in the local limit

Similar to the strict model case, we begin with the study of the states in the single-cluster limit. Here the non-interacting part of the Hamiltonian is given by the $(0,0)$ column of Tab. I (note that of course just the NN t enters in that limit). Thus not only $t < 0$ now holds, but also the symmetry of the cluster Hamiltonian is lowered at finite doping because of the inequivalent Co sites. Our aim is not to discuss the energy spectrum in the cluster limit at each doping level in full detail. Only the major differences to the high-symmetry ($t > 0$) model case treated before shall be elucidated.

The spectrum of the cluster eigenstates at $x=2/3$ for $U=0$ eV is shown in Fig. 10. The loss of degeneracy due to the lower symmetry is obvious. In general, because of the sign change in t , the spectrum is more or less mirrored compared to the ($t > 0$) model case. While for the latter, low-particle sectors were energetically favoured,

here the six-particle singlet at ~ -3.37 eV is the lowest state in energy. Thereafter five-particle doublets follow in energy, which will turn out to be important in the itinerant lattice problem discussed in the next section. As an additional generic difference to $t>0$ the particle sectors tend to group, larger fillings at lower energies due to the reduced number of possible hopping processes which are now penalized by energy cost. On the contrary, for the ($t>0$) case the particle sectors are distributed over the whole range of the spectrum for $U=0$ eV (cf. Fig. 2).

Focusing on the four-particle sector which turned out to be important in the doped ($t>0$) case, it is observable that now a singlet is forming the lowest energy state³⁹. Remember that the onset of FM order for $t>0$ from the local viewpoint may be associated with the dominance of the ground-state triplet. Moreover the Fock-space decomposition of the four-particle ground state, shown in Fig. 11, is far more complex for the singlet than for the former triplet (see Fig. 3). The ground-state singlet cannot be polarized. To get a polarization, the cluster with four electrons would have to be excited, e.g., to the named triplet state. But even in the non-interacting case this would cost an energy of about 0.3eV.

The emerging cluster spectrum in the interacting case ($U=5$ eV) for the Hamiltonian associated with the filling $x=2/3$ is shown in Fig. 12. Now the lowest energy state stems from the three-particle sector and its highly degenerated doublets and quadruplets. It is followed by a number of two-particle states and the overall tendency to group states is enforced. Of course by including a Hubbard $U=5$ eV the many-particle sectors become energetically also costly compared to the non-interacting

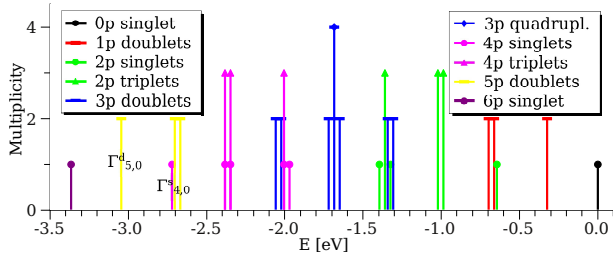


FIG. 10: (Color online) Energy spectrum of the cluster limit of the LDA-derived model Na_xCoO_2 for $x=2/3$ and $U=0$ eV.

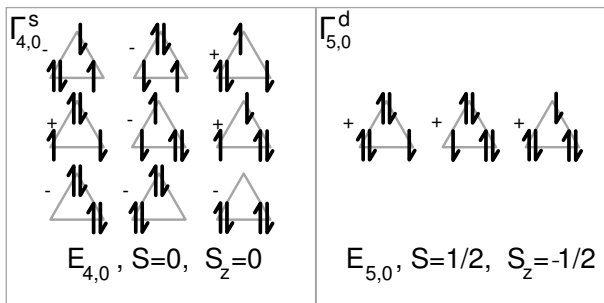


FIG. 11: Relevant cluster multiplets for the paramagnetic LDA-derived model.

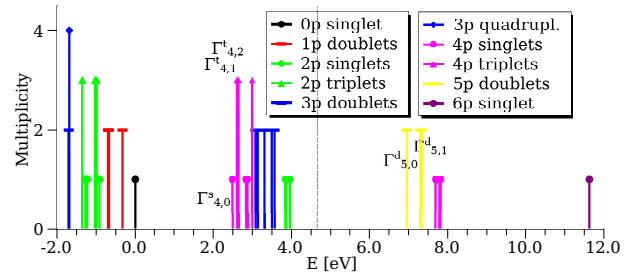


FIG. 12: (Color online) Same as Fig. 10 but for $U=5$ eV.

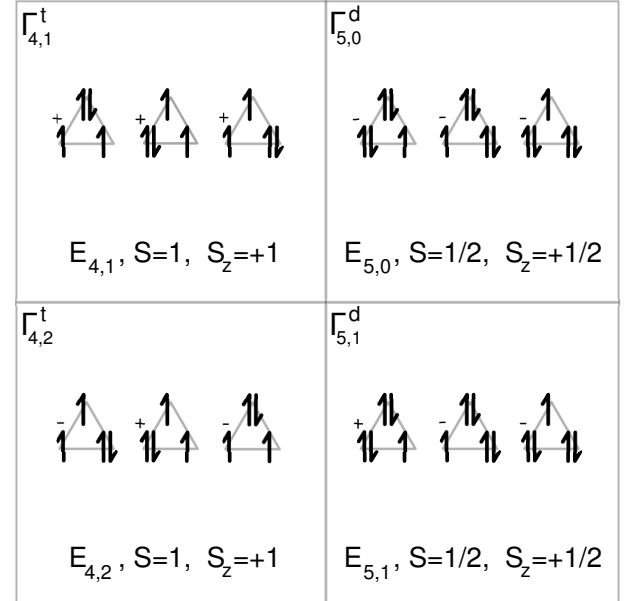


FIG. 13: Relevant cluster multiplets for the ferromagnetic LDA-derived model.

case. In the four-particle sector, the singlet is still lowest in energy, but the triplet draws near, the energy gap becomes smaller by about a factor of three. That means the interacting Na_xCoO_2 triangle with a filling of four electrons is still less polarizable in the local cluster limit than the triangle with $t>0$, but the local Coulomb repulsion naturally tends to support tendencies towards spin polarization. As shall be seen in the itinerant problem, the following three particle doublets and other singlets can be neglected. Next in energy and easy to polarize due to a single free spin on the cluster is the degenerated five-particle doublet. As shown in Fig. 13 it resembles the structure of the easy to polarize four-particle triplet from the ($t>0$) case. In other words, while from this local viewpoint the ($t>0$) case exhibits susceptibility towards FM order at smaller doping associated with the four-particle triplet, the Na_xCoO_2 ($t<0$) case shows such tendencies only at higher doping connected to the five-particle doublet.

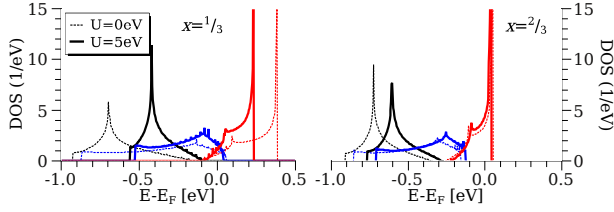


FIG. 14: (Color online) QP spectral function of PM Na_xCoO_2 at $x=1/3$ and $x=2/3$. The splitting into three parts, respectively, is due to the cluster description (see text).

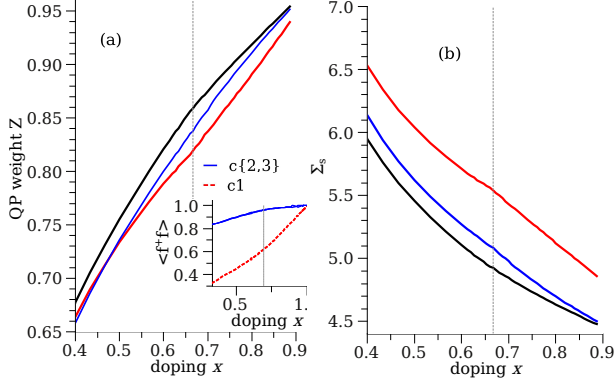


FIG. 15: (Color online) Doping-dependent quasiparticle weight (a) and local self-energy (b) for PM Na_xCoO_2 , given in the eigenbasis of the QP operator $\langle f^\dagger f \rangle$, i.e., the orbital density matrix. Close to $x=2/3$ the red/grey orbital, corresponding to the strong filling-dependent state in the inset (ψ_{c_1} , also red/grey) shows a stronger renormalisation than the other two (blue/dark).

B. Lattice modeling

The central aim of this subsection is to investigate the in-plane magnetic behavior of sodium cobaltate close to zero temperature with doping x . It is known that eventually the CoO_2 planes couple antiferromagnetically (A-type AFM order). Here we want to address the question why Na_xCoO_2 displays different in-plane magnetic correlations with doping and finally FM magnetic order for $3/4 < x < 0.9$. In this respect the mean-field RISB method allows for the possibility to stabilize paramagnetic as well as symmetry-broken ferromagnetic phases for the realistic Hamiltonian (eq. (2))⁴⁹. For instance, a FM phase may be set up via initial spin-different lagrange multipliers and this lowered symmetry is self-consistently reproduced at saddle-point convergence if such a phase is (locally) stable. $U=5$ eV was set for the interacting case and we concentrate on dopings $x \geq 1/3$ where the a_{1g} -like modeling should be well justified. Note that now of course also the LDA-derived hoppings beyond NN distance come into play, thus a one-to-one comparison with the NN-only model has to be taken with caution.

The QP spectral function in Fig. 14 shows the decomposition into three parts due to the cluster description. The different parts represent the K-integrated spectral

weight of the resulting supercell bands. They naturally add up to the known a_{1g} -like cobaltate dispersion^{6,42} in the non-interacting case. Note that we only consider the 2D dispersions in K-space. As expected from the doping levels, the overall renormalization is weakened at $x=2/3$ compared to the $x=1/3$ case. In the higher doping regime the spectral weight strongly increases close to the additional van-Hove singularity, which could point to the relevance of Stoner-like mechanisms for the onset of in-plane FM order.

The variation of the QP weight Z and the static self-energy part Σ_s (see eq. (10)) with x is plotted in Fig. 15. We display the quantities in the eigenbasis of the cluster orbital density matrix $\langle f^\dagger f \rangle$ of the correlated problem in order to make the point that the usual site-basis may not always be the most adequate one. Note that resulting eigenstates do *not* directly correspond to the spectral-weight parts from Fig. 14, since the latter stem from a diagonalization at each K-point. It is seen that two of the eigenstates of $\langle f^\dagger f \rangle$, $\psi_{c_{2,3}}$, are highly occupied whereas the filling of the remaining effective orbital ψ_{c_1} shows strong doping dependence. $Z(x)$ and $\Sigma_s(x)$ exhibit the strongest differences among those states around $x \sim 2/3$, pointing towards dominant inter-site correlations. Represented in the site basis, the splitting of the diagonal elements of $Z(x)$ and $\Sigma_s(x)$ is diminished. However on the present modeling level the discrepancy between the effective orbitals, aside from the filling behavior, is not significant. The overall degree of correlation with $Z \sim 0.82-0.86$ in this designated doping regime is still modest. We will elaborate on this point in section V.

Figure 16 shows the pair-averaged spin-correlation functions $\langle S_i S_j \rangle$ between Co sites i, j on the 3-site cobaltate cluster. Already the non-interacting treatment shows substantial AFM correlations for small doping in the PM phase, which are strongly reinforced by the Hubbard U . The latter is easily understandable from the relevant superexchange mechanism close to half filling ($x=0$). But on the other hand interestingly the AFM correlations are more significantly suppressed for finite U at large x . At $x \sim 2/3$ there is a clear crossover in these short-range correlations visible between interacting and non-interacting case. Though a generally diminished $\langle S_i S_j \rangle$ amplitude at larger doping is reasonable from the sole reduction of the local magnetic moments, this crossover remains remarkable. Hence the spin correlations in the correlated regime show highly non-trivial behavior with doping. In addition, at $x \sim 0.61$ indeed a long-range ordered FM metal may be stabilized. The metallic cluster magnetization of that phase exhibits linearly decreasing behavior with doping, with subtle convergence properties for $x > 0.9$ concerning the K-point integration with smearing methods.

Figures 17 and 18 show the relevant slave-boson amplitudes for the competing phases with doping x . In Fig. 17 only the paramagnetic phase is investigated. Since the system is in a high-doping regime, multiplets from the four-, five- and six-particle sector play the dominant

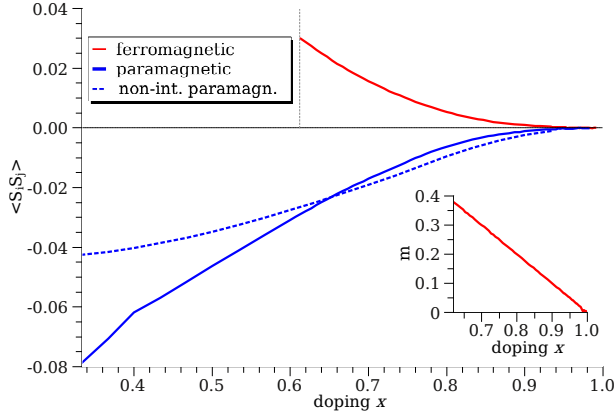


FIG. 16: (Color online) Doping-dependent spin correlation function on the triangular cluster for the PM interacting (blue/dark full) and non-interacting (blue/dark dashed) phase as well as the FM phase (red/grey full). Inset: averaged cluster magnetization with x .

role. Starting below $x \sim 0.4$, the four-particle singlet is strongest, in line with the ongoing NN-AFM correlations there. At $x \sim 0.52$ the five-particle doublets however overrun the four-particle-singlet weight and reach a maximum at around $x = 0.69$. Hence at $x \sim 2/3$, the probability to find the system in one of the two doublet states is about 25% each. As the doping increases even further the six-particle singlet, corresponding to completely filled cluster becomes of course dominant. As expected, the six-particle singlet is much stronger occupied in the non-interacting case for constant x . However also the occupation of the doublet is smaller for $U = 0$ eV, while the four-particle singlet gains weight in the doping range $x > 0.44$. This corresponds to an enhanced establishment of a net spin on the triangular cluster with sizeable Hubbard U , which gives the trend towards ferromagnetic behavior on the lattice. At small doping below $x \sim 0.44$, the singlet is favored by interaction, underlining the AFM tendencies. It is interesting to note that the dominant maximum of the five-particle doublet around $x \sim 0.7$ only little depends on the influence of the hopping terms beyond NN. Albeit the latter are responsible for the van-Hove singularity close to the upper band edge for $t < 0$, a RISB calculation with only NN t (fixed here to the value $t = -135$ meV) results mainly in the enhancement of the four-particle singlet weight (see inset of Fig. 17). Thus the more distant hoppings indeed strengthen the trend towards in-plane ferromagnetism, but it is questionable if this is the only explanation for the eventual FM order.

The occupations of the slave-boson states in the PM and the FM phase are compared in Fig. 18. In the ferromagnetic phase, the degeneracy of the dominant five-particle doublets is lifted with the favored $S_z = 1/2$ one showing a prominent maximum at $x \sim 0.68$. The probability to find the system in that state amounts to roughly 50%. Note that the four-particle ground-state singlet is not occupied at all in the FM phase, instead triplet

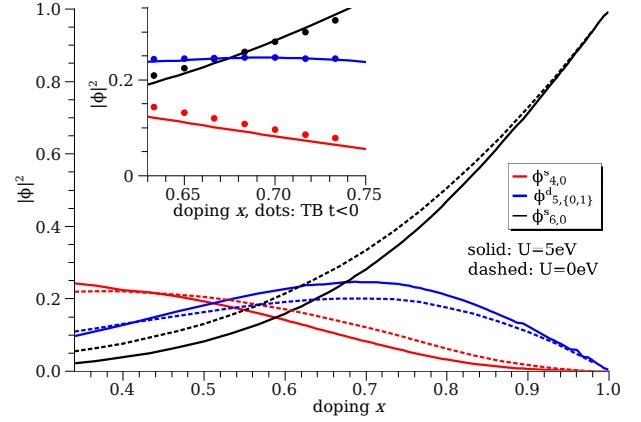


FIG. 17: (Color online) Doping-dependent relevant slave-boson amplitudes for the interacting ($U = 5$ eV) and non-interacting PM phase within the LDA-derived Na_xCoO_2 model. Inset: Comparing interacting cases with complete dispersion (full lines) and only NN hopping (dots) around $x \sim 0.7$.

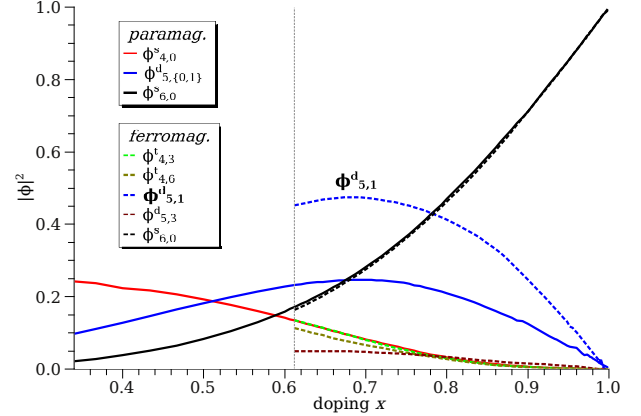


FIG. 18: (Color online) As Fig. 17 but now comparing interacting PM and FM phases.

states with $S_z = +1$ from that particle sector display some weight.

In order to map out the actual stability ranges of the PM and FM phase, the doping-dependent free energy has to be studied. Accordingly Fig. 19 shows the respective curves obtained from the saddle-point solution of the RISB free-energy functional⁸⁴. Be aware that our present discussion is limited to the 2D limit of Na_xCoO_2 and that very general stability statements can of course only be made for the full 3D case⁴⁹. Note also that a *full* FM order of the 3D lattice can truly not be stabilized in the RISB treatment of our model cobaltate. One may observe in Fig. 19 that the FM phase is only (meta)stable around $x \sim 2/3$. Above $x \sim 0.7$ it becomes locally stable, but as revealed by the tie-line construction, globally a mixed PM-FM phase is the thermodynamic stable solution in the range $0.62 < x < 3/4$. This first-order scenario for the onset of magnetic order is substantiated by the experimental findings of A-type AFM ordered phases starting

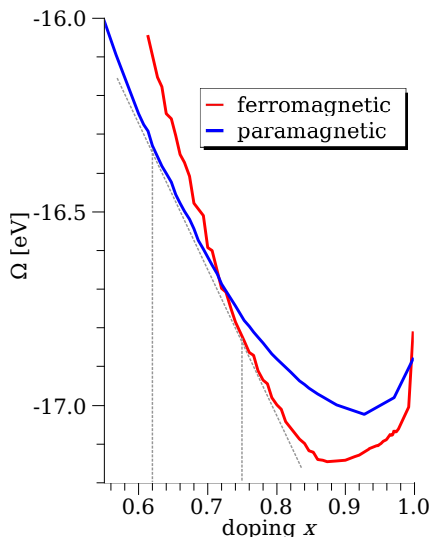


FIG. 19: (Color online) RISB free energy for the PM (blue/dark) and FM (red/grey) phase. There is a region of coexistence ranging from $x_a \approx 0.62$ to $x_b \approx 3/4$ obtained from the tie-line construction.

at $x \sim 3/4$ with a small but still sizeable finite magnetic moment (in line with our theoretical values). Moreover the peculiar behavior in the given doping range, especially around $x \sim 0.7$, was elucidated in several experimental works^{67–70}. The RISB FM free-energy curve displays a minimum close to $x > 0.9$. While in experiment the magnetic order is lost for $x > 0.9$, our mean-field solution in the 2D limit still allows for in-plane FM order up to the band-insulating regime. But the obtained numerical solutions in that doping regime are rather fragile and temperature effects (somehow mimicked in the present RISB implementation via the smearing in the K-point integration) are very effective in easily destroying a simple thermodynamic phase behavior. Remember that experimentally close to $x = 1$ strong tendencies towards phase separation are seen (e.g. Ref. 71 and references therein), which may also be detected theoretically⁴⁹.

Since the employed cellular-cluster calculations are numerically rather costly, the question arises if the thermodynamic behavior from Fig. 19 may also be retrieved from a single-site point of view. Therefore we studied two alternative approaches, namely the multi-single-site solution of our established cobaltate model and a true single-site model derived from the LDA band structure of the single Co site unit cell of NaCoO_2 . Note that the former model corresponds to the neglect of inter-site self-energies, however keeping site-dependent self-energies in the cluster unit cell. The calculations revealed that the multi-single-site approach yields nearly identical free-energy curves in the relevant doping regime, with deviations becoming sizeable only at smaller x closer to the half-filled regime. Still, quantitatively the cluster free-energy remains always lower by a few ten meV. On the other hand the true single-site model showed similar ten-

dencies, i.e., PM phase at intermediate and FM phase at high doping, but resulted in rather different phase boundaries not matchable with experimental findings. Hence inter-site self-energies seem not essential for the *overall integrated thermodynamic* behavior on the present level of modeling (but surely are for the detailed electronic signatures). Yet a non-local description in the sense of site-dependent self-energies in enlarged supercell descriptions is believed to be crucial for the energetics of sodium cobaltate.

V. STRONGLY DOPED SODIUM COBALTATE WITH EXTENDED COULOMB INTERACTIONS

So far the modeling was concentrated on the generic doping dependence of the correlation effects within a single-layer approximation to the range $1/3 \leq x \leq 1$. In this last section we want to elaborate on the modeling for the doping regime around $x \sim 2/3$, which appears distinguished because of its strong thermoelectric response as well as its magnetic behavior in line with the apparent phase competitions discussed in section IV. Hence a more refined structural modeling taking also into account the observed charge ordering phenomena for $x > 0.5$ should shed more light upon the physics in this region of the phase diagram. Recent experimental findings revealed the possibility of a kagomé-lattice imprint in the CoO_2 layers at $x = 2/3$ due to Na-ordering driven charge order⁴⁸ and we want to build up a more subtle realistic cobaltate model on this proposal. To include the effect of a charge-ordered background the inter-site Coulomb interaction V is now vital. As will be shown, therewith one is also in the position to finally describe the strong mass-renormalization effects in this high-doping regime, which were out of reach in the local- U only modeling (cf. Fig. 15).

Figure 20 shows the Na-decorated CoO_2 layer of an approximant to the rather complex true $\text{Na}_{2/3}\text{CoO}_2$ lattice structure detected in Ref. 48 (incorporating 88 atoms in the unit cell). The former structure has four in-plane Co sites in the unit cell, where one of the sites (Co(1)) has a Na ion on top, i.e., in the Na(1) position, and the other sodium ions occupy Na(2) positions close to the remaining Co(2) sites. Thereby the approximant is a simple approach to mimic the key property of the original structure, namely a kagomé-lattice imprint if one assumes the Co(1) sites to be formally in the charge-blocked Co^{3+} state⁴⁸. Albeit a simple LDA calculation surely does not yield a strong charge-ordered pattern, we proceed in constructing an effective kagomé lattice model for $\text{Na}_{2/3}\text{CoO}_2$ by projecting the resulting band structure onto a_{1g} -like Wannier functions centered *only* at the Co(2) sites. Since in addition we want to incorporate now also the full staggered 3D character we use the Co(2) sites in two adjacent CoO_2 layers. Hence we end up with a six-dimensional model where, respectively,

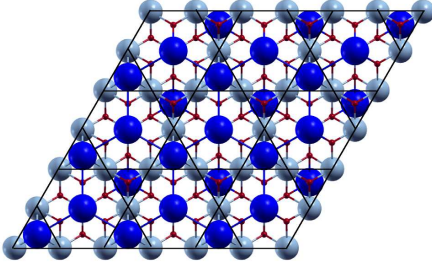


FIG. 20: (Color online) Top view on the Na decorated CoO_2 layer of the utilized crystal approximant to the experimentally detected kagomé-lattice imprint⁴⁸. Sodium atoms are marked blue/dark, cobalt atoms grey and oxygen atoms red/lightgrey. The resulting effective kagomé lattice is sketched via dark lines.

three Wannier functions are again located on an in-plane triangle cluster as a basis for an effective kagomé lattice (cf. Fig. 20). Note that this is a simple approximation to an actual blocking of the Co(1) sites through projecting out the explicit hoppings degrees of freedom associated with orbitals located on those sites. From this derivation of the realistic Hamiltonian the NN hopping amounts to $t = -152$ meV, i.e. is slightly larger than for the initial triangular lattice model at $x = 2/3$ (cf. Tab. I). The NN inter-layer hopping amounts now to $t_{\perp} = 9$ meV, i.e., is somewhat smaller than in the pure triangular case. Thus the 2D character, again loosely defined via t_{\perp}/t , is reinforced for the effective kagomé lattice.

In the following the emphasis is still on the physics within a single CoO_2 layer and in the PM phase. However the description within the full 3D structure, allowing here for inter-layer resolution, is capable of revealing not only the experimentally-observed bi-layer splitting in the correlated regime. In addition we now easily may stabilize the A-type AFM order in the RISB calculations. While V is varied to look for the influence of the inter-site Coulomb term, the Hubbard U remains fixed to $U = 5$ eV. Since the physics is now studied on an effective lattice where the supposedly blocked Co^{3+} states have been projected out, the nominal filling on that lattice is of course not identical to the original doping level x . Its easily shown that the latter value is related to the effective doping x_{eff} for the given kagomé problem through $x_{\text{eff}} = (4x - 1)/3$.

The liberty is taken to allow for a stability of the effective kagomé structure also for dopings somewhat larger than $x = 2/3$. Since it is known that the charge ordering persists in that region, the use of the ($x = 2/3$)-structure with adjusted doping level may serve as a suitable first approximation. In Fig. 21 the orbital filling and the QP weight Z of the eigenstates of $\langle f^{\dagger}f \rangle$ for the dopings $x = 2/3, 3/4, 4/5$, i.e. $x_{\text{eff}} = 5/9, 2/3, 11/15$, are displayed. The transformation to the given eigenbasis becomes now vital since its is easily observed that the inter-site V has a rather strong influence on the observables. For $x_{\text{eff}} = 2/3$ the effective kagomé lattice is in the ordering regime of a

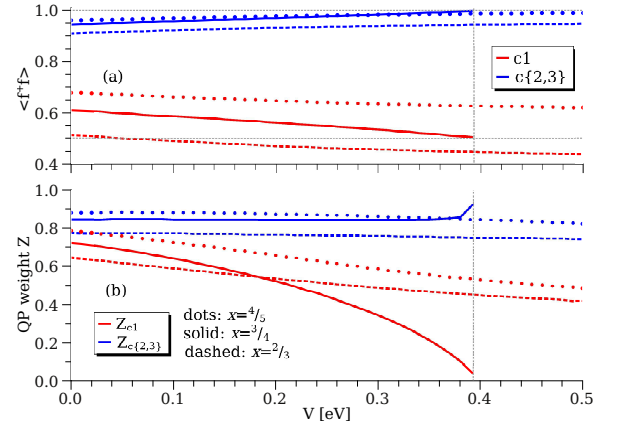


FIG. 21: (Color online) Occupations (a) and QP weight (b) for the extended cobaltate Hubbard model on the effective kagomé lattice with increasing V in the eigenbasis of the cluster orbital density matrix.

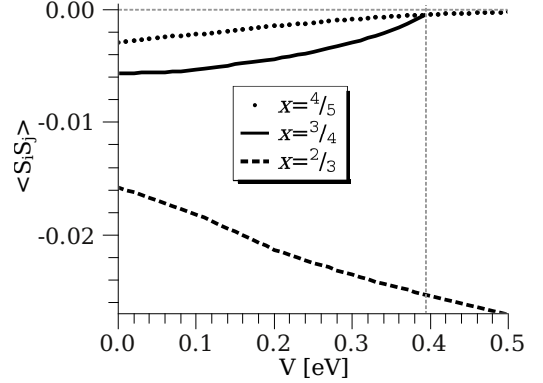


FIG. 22: (Color online) Inter-site spin correlations on the triangular cluster of the the effective kagomé lattice for the three different doping levels.

charge-density-wave (CDW) instability on a lattice with triangular coordination^{60,72–74}. In the present study, this instability is not driven by a charge localization on the lattice sites i , but in the eigenstates c of the triangular cluster. The strongly renormalized state c_1 in Fig. 21 corresponds locally to a symmetrical cluster eigenstate of the form $\psi_c = A \sum_{i=1}^3 \psi_i$ (note that $t < 0$ inverts the bonding-antibonding energy hierarchy), where the amplitude A is identical for all a_{1g} -like site-centered states and independent of V . The remaining two cluster eigenstates are degenerate with non-trivial linear combination of the site-centered states. Note that this result may serve as a natural explanation for the findings of small quasiparticle weights in the high doping regime^{75–77}.

Thus for large V and $x_{\text{eff}} \sim 2/3$ the system is unstable against a resonating-valence-bond- (RVB) like CDW phase. Because of the cluster choice within the cellular description, that phase still breaks translational invariance. At the actual $x = 2/3$ level, the discrimination between the quasiparticle weight of the respective eigenstates is still visible, yet the strong signature is lost.

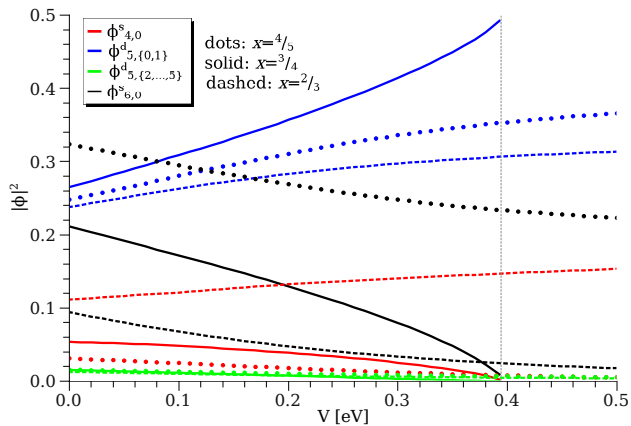


FIG. 23: (Color online) Slave-boson amplitudes of selected multiplet states on the triangular cluster of the effective kagomé lattice for the three different doping levels.

The critical value $V_c \sim 0.4$ eV for the metal-insulator transition at commensurate filling is perfectly reasonable for the cobaltate system. Concerning the in-plane spin correlations, Fig. 22 remarkably shows that the inter-site V has a qualitatively different effect on the various dopings. While V for $x_{\text{eff}}=5/9$ ($x=2/3$) strengthens the AFM tendencies, at $x_{\text{eff}}=2/3$ ($x=3/4$) the AFM character is substantially weakened, with a clear trend towards FM correlations. For $x_{\text{eff}}=11/15$ ($x=4/5$) the NN-AFM correlations are already rather weak in the PM phase. Interestingly, $x_{\text{eff}} \sim 2/3$ just corresponds to the actual doping value $x=3/4$ of the full triangular lattice where the onset of in-plane FM order is found experimentally. In this context it is essential to note that there are very strong hints that the maximum experimental Curie-Weiss susceptibility is indeed not at $x=2/3$ but closer to the $x=3/4$ doping level^{13,78}. Hence besides the general thermodynamic considerations presented in the former section, the explicit inclusion of realistic charge ordering effects also points to the onset of in-plane FM order at $x \sim 3/4$ with a unique underlying electronic phase.

Considering once again the slave-boson amplitudes of the local cluster multiplets for the investigated doping levels, Fig. 23 renders it obvious that for $x=3/4$ the five-particle doublets are strongly favored by V . On the other hand for $x=2/3$ that multiplet, though still dominating, has to cope with a still sizeable occupation of the four-particle singlet state. Therefrom, the enhanced AFM tendencies in the latter instance compared to the $V=0$ eV case are understandable from the local cluster perspective. This four-particle singlet state becomes even more suppressed for $x=4/5$, where experimentally already the in-plane FM phase is established.

VI. CONCLUSIONS

In this paper we employed the RISB mean-field formalism to approach the sodium cobaltate system at larger

doping by combining realistic LDA dispersions with tailored many-body model Hamiltonians in a cellular-cluster scheme. Due to the intriguing sodium order with doping, a realistic, numerically feasible modeling for a large part of the phase diagram asks for a simple, but still non-trivial approximate treatment of the structural details. We showed that non-local correlation effects (at least in a short-range regime) are indispensable to account for the phase behavior in the magnetically active region $x > 0.5$. Site-dependent self-energies, triggered by the sodium ordering, are at minimum needed to allow for reasonable insight into the physics of Na_xCoO_2 .

Emphasis was taken to study the interplay between band-structure effects and local cluster correlations in the investigation of the highlighting magnetic properties. It became clear that though the van-Hove singularity at the upper band edge (due to long-range hopping terms) is a vital ingredient, the apparent many-body correlations on the frustrated lattice are an additional relevant source for the enhanced susceptibilities. In this respect, the slave-boson amplitudes for the triangular cluster multiplets proved to be valuable observables to substantiate the latter statement. For instance, FM tendencies for Na_xCoO_2 ($t < 0$) close to $x=2/3$ in contrast to the strong FM susceptibility for $t > 0$ close to $x=1/3$ may directly be connected to the local triangular cluster correlations. The relevance of five-particle doublet cluster states in the neighborhood of $x=2/3$ should motivate a different viewpoint on the basic entities of the cobaltates. Namely, approaching the magnetic properties in this doping regime from a larger (not necessarily triangular) cluster perspective appears superior to the incommensurate single-site starting point.

Aside from the simplified Stoner approach there are various more specialized considerations concerning ferromagnetism in Hubbard(-like) models, e.g., ideas based on Nagaoka's theorem⁷⁹, Kanamori's criterion⁸⁰ in the low-density regime or ring-exchange mechanisms relevant for triangular plaquettes^{81,82}. A very direct connection to such model ideas is complicated because of the difficult structural facts, however it may well be that certain aspects therefrom also apply to sodium cobaltates⁸³.

Our calculations revealed that the doping region $0.6 < x < 3/4$ is highly susceptible for magnetic phase separation, pointing towards a first-order-transition scenario for the onset of the A-type AFM order. These theoretical findings are in accordance with many experimental studies in that region⁶⁷⁻⁷⁰, which, e.g., revealed hints for disorder-induced non-Fermi-liquid behavior with possibly underlying quantum Griffiths phases⁷⁰. The region close to the band-insulating $x=1$ limit appears interesting for several reasons, since it is expected that a minimal hole doping of that state⁴⁴ will result in nontrivial charge susceptibilities compared to standard weakly correlated systems. However the simple structural model prohibits at this level detailed deeper investigations.

The final study on the ambitious modeling of dopings close to $x=2/3$ based on the more elaborate effective

kagomé lattice within a charge-ordered background seem rather fruitful concerning the understanding of the interplay between the charge and spin degrees of freedom. It showed that the charge ordering may be efficient in singling out distinct phases that can give rise to enhanced FM tendencies at specific dopings. This viewpoint delivers a rather natural possible explanation not only for the onset of FM order *above* $x=2/3$, but provides a clear-cut interpretation for the strong correlations in that doping regime. The blocking of some of the charge not solely reduces the effective hopping. It also gives rise to sizeable inter-site Coulomb interactions that strongly renormalize the remaining half-filled effective state emerging from the neighborhood to an fluctuating CDW instability on the still accessible lattice sites. This general idea carries over to the specific kagomé pattern and may be generalized to the even higher doping regions by thinking of *larger* clusters with *more* blocked sites. Future work shall also be focused on the understanding of the spectral properties of such phases, probably also relevant in the misfit cobaltates, in order to touch base with already available angle-resolved photoemission (ARPES) data^{37,38,75–77}. In this respect, magnetic and ARPES measurements already suggested a fluctuating character

of a hidden collective CDW-like instability^{23,75}, possibly driven by long-range Coulomb interactions.

In summary, because of its compelling physical richness the sodium cobaltate system serves as a demanding testing ground for the nowadays available realistic many-body tools. Non-local correlations effects naturally show up in Na_xCoO_2 and this shall stimulate further work on schemes to handle those as well as on many-body Hamiltonians beyond the standard Hubbard model.

Acknowledgments

The authors are indebted to Henri Alloul, Veronique Brouet, Daniel Grieger and Oleg Peil for helpful discussions. Financial support from the DFG-SPP 1386 is acknowledged. This research was supported in part by the National Science Foundation under Grant No. NSF PHY05-51164. Computations were performed at the local computing center of the University of Hamburg as well as the North-German Supercomputing Alliance (HLRN) under the grant hhp00026.

-
- ¹ H. T. Diep, *Frustrated Spin Systems* (World Scientific Publishing Company, 2005).
- ² C. Lacroix, J. Phys. Soc. Jpn. **79**, 011008 (2010).
- ³ Y. Kamihara, T. Watanabe, M. Hirano, and H. Hosono, J. Am. Chem. Soc. **130**, 3296 (2008).
- ⁴ Q. Si and E. Abrahams, Phys. Rev. Lett. **101**, 076401 (2008).
- ⁵ F. Krüger, S. Kumar, J. Zaanen, and J. van den Brink, Phys. Rev. B **79**, 054504 (2009).
- ⁶ F. Lechermann, S. Biermann, and A. Georges, Progress of Theoretical Physics Supplement **160**, 233 (2005).
- ⁷ D. Pillay, M. D. Johannes, I. I. Mazin, and O. K. Andersen, Phys. Rev. B **78**, 012501 (2008).
- ⁸ C. A. Marianetti, K. Haule, and O. Parcollet, Phys. Rev. Lett. **99**, 246404 (2007).
- ⁹ G.-T. Wang, X. Dai, and Z. Fang, Phys. Rev. Lett. **101**, 066403 (2008).
- ¹⁰ A. Liebsch and H. Ishida, Eur. Phys. J. B **61**, 405 (2008).
- ¹¹ A. Bourgeois, A. A. Aligia, and M. J. Rozenberg, Phys. Rev. Lett. **102**, 066402 (2009).
- ¹² K. Takada, H. Sakurai, E. Takayama-Muromachi, F. Izumi, R. A. Dilanian, and T. Sasaki, Nature **422**, 53 (2003).
- ¹³ M. L. Foo, Y. Wang, S. Watauchi, H. W. Zandbergen, T. He, R. J. Cava, and N. P. Ong, Phys. Rev. Lett. **92**, 247001 (2004).
- ¹⁴ I. R. Mukhamedshin, H. Alloul, G. Collin, and N. Blanchard, Phys. Rev. Lett. **94**, 247602 (2005).
- ¹⁵ G. Lang, J. Bobroff, H. Alloul, G. Collin, and N. Blanchard, Phys. Rev. B **78**, 155116 (2008).
- ¹⁶ Y. Wang, N. S. Rogado, R. J. Cava, and N. P. Ong, Nature **423**, 425 (2003).
- ¹⁷ T. Fujimoto, G.-Q. Zheng, Y. Kitaoka, R. L. Meng, J. Cmaidalka, and C. W. Chu, Phys. Rev. Lett. **92**, 047004 (2004).
- ¹⁸ M. Yokoi, T. Moyoshi, Y. Kobayashi, M. Soda, Y. Yasui, M. Sato, and K. Kakurai, J. Phys. Soc. Jpn. **74**, 3046 (2005).
- ¹⁹ S. Kawasaki, T. Motohashi, K. Shimada, T. Ono, R. Kanno, M. Karppinen, H. Yamauchi, , and G.-Q. Zheng, Phys. Rev. B **79**, 220514 (2009).
- ²⁰ C. de Vaulx, M.-H. Julien, C. Berthier, S. Hébert, V. Pralong, and A. Maignan, Phys. Rev. Lett. **98**, 246402 (2007).
- ²¹ P. Mendels, D. Bono, J. Bobroff, G. Collin, D. Colson, N. Blanchard, H. Alloul, I. Mukhamedshin, F. Bert, A. Amato, et al., Phys. Rev. Lett. **94**, 136403 (2005).
- ²² J. Sugiyama, H. Itahara, J. H. Brewer, E. J. Ansaldo, T. Motohashi, M. Karppinen, and H. Yamauchi, Phys. Rev. B **67**, 214420 (2003).
- ²³ T. Motohashi, R. Ueda, E. Naujalis, T. Tojo, I. Terasaki, T. Atake, M. Karppinen, and H. Yamauchi, Phys. Rev. B **67**, 064406 (2003).
- ²⁴ A. T. Boothroyd, R. Coldea, D. A. Tennant, D. Prabhakaran, L. M. Helme, and C. D. Frost, Phys. Rev. Lett. **92**, 197201 (2004).
- ²⁵ Y. Ihara, K. Ishida, C. Michioka, M. Kato, K. Yoshimura, H. Sakurai, and E. Takayama-Muromachi, J. Phys. Soc. Jpn. **73**, 2963 (2004).
- ²⁶ H. Sakurai, N. Tsujii, and E. Takayama-Muromachi, J. Phys. Soc. Jpn. **73**, 2393 (2004).
- ²⁷ S. P. Bayrakci, I. Mirebeau, P. Bourges, Y. Sidis, M. Endlerle, J. Mesot, D. P. Chen, C. T. Lin, and B. Keimer, Phys. Rev. Lett. **94**, 157205 (2005).
- ²⁸ L. M. Helme, A. T. Boothroyd, R. Coldea, D. Prabhakaran, A. Stunault, G. J. McIntyre, and N. Kernavanois, Phys. Rev. B **73**, 054405 (2006).

- ²⁹ G. J. Shu, A. Prodi, S. Y. Chu, Y. S. Lee, S. Sheu, and F. C. Chou, *Phys. Rev. B* **76**, 184115 (2007).
- ³⁰ T. F. Schulze, M. Brühwiler, P. S. Häfziger, S. M. Kazakov, C. Niedermayer, K. Mattenberger, J. Karpinski, and B. Batlogg, *Phys. Rev. B* **78**, 205101 (2008).
- ³¹ D. Singh, *Phys. Rev. B* **61**, 13397 (2000).
- ³² D. Singh, *Phys. Rev. B* **68**, 020503 (2003).
- ³³ M. D. Johannes, I. I. Mazin, and D. J. Singh, *Phys. Rev. B* **71**, 214410 (2005).
- ³⁴ N. L. Wang, P. Zheng, D. Wu, Y. C. Ma, T. Xiang, R. Y. Jin, and D. Mandrus, *Phys. Rev. Lett.* **93**, 237007 (2004).
- ³⁵ T. Valla, P. D. Johnson, Z. Yusof, B. Wells, Q. Li, S. M. Loureiro, R. J. Cava, M. Mikami, M. Y. Y. Mori, and T. Sasaki, *Nature* **417**, 627 (2002).
- ³⁶ M. Z. Hasan, Y.-D. Chuang, D. Qian, Y. W. Li, Y. Kong, A. Kuprin, A. V. Fedorov, R. Kimmberling, E. Rotenberg, K. Rossnagel, et al., *Phys. Rev. Lett.* **92**, 246402 (2004).
- ³⁷ H.-B. Yang, Z. Wang, and H. Ding, *J. Phys.: Condens. Matter* **19**, 355004 (2007).
- ³⁸ J. Geck, S. V. Borisenko, H. Berger, H. Eschrig, J. Fink, M. Knupfer, K. Koepernik, A. Koitzsch, A. A. Kordyuk, V. B. Zabolotnyy, et al., *Phys. Rev. Lett.* **99**, 046403 (2007).
- ³⁹ J. Merino, B. J. Powell, and R. H. McKenzie, *Phys. Rev. B* **73**, 235107 (2006).
- ⁴⁰ H. Rosner, S.-L. Drechsler, G. Fuchs, A. Handstein, A. Wälte, and K.-H. Müller, *Braz. J. Phys.* **33**, 718 (2003).
- ⁴¹ M. D. Johannes, D. A. Papaconstantopoulos, D. J. Singh, and M. J. Mehl, *Europhys. Lett.* **68**, 433 (2004).
- ⁴² K. W. Lee, J. Kunes, and W. E. Pickett, *Phys. Rev. B* **70**, 045104 (2004).
- ⁴³ M. M. Korshunov, I. Eremin, A. Shorikov, V. I. Anisimov, M. Renner, and W. Brenig, *Phys. Rev. B* **75**, 094511 (2007).
- ⁴⁴ M. Gao, S. Zhou, and Z. Wang, *Phys. Rev. B* **76**, 180402 (2007).
- ⁴⁵ L. Nordheim, *Ann. Phys. (Leipzig)* **9**, 607 (1931).
- ⁴⁶ C. A. Marianetti and G. Kotliar, *Phys. Rev. Lett.* **98**, 176405 (2007).
- ⁴⁷ J. O. Haerter, M. R. Peterson, and B. S. Shastry, *Phys. Rev. Lett.* **97**, 226402 (2006).
- ⁴⁸ H. Alloul, I. R. Mukhamedshin, T. A. Platova, and A. V. Dooglav, *Europhys. Lett.* **85**, 47006 (2009).
- ⁴⁹ F. Lechermann, *Phys. Rev. Lett.* **102**, 046403 (2009).
- ⁵⁰ T. Li, P. Wölfle, and P. J. Hirschfeld, *Phys. Rev. B* **40**, 6817 (1989).
- ⁵¹ F. Lechermann, A. Georges, G. Kotliar, and O. Parcollet, *Phys. Rev. B* **76**, 155102 (2007).
- ⁵² D. Galanakis, T. D. Stanescu, and P. Phillips, *Phys. Rev. B* **79**, 115116 (2009).
- ⁵³ P. A. Lee, N. Nagaosa, and X.-G. Wen, *Rev. Mod. Phys.* **78**, 17 (2006).
- ⁵⁴ N. Marzari and D. Vanderbilt, *Phys. Rev. B* **56**, 12847 (1997).
- ⁵⁵ I. Souza, N. Marzari, and D. Vanderbilt, *Phys. Rev. B* **65**, 035109 (2001).
- ⁵⁶ B. Meyer, C. Elsässer, F. Lechermann, and M. Fähnle, *FORTTRAN 90 Program for Mixed-Basis-Pseudopotential Calculations for Crystals*, Max-Planck-Institut für Metallforschung, Stuttgart (unpublished).
- ⁵⁷ S. G. Louie, K. M. Ho, and M. L. Cohen, *Phys. Rev. B* **19**, 1774 (1979).
- ⁵⁸ Q. Huang, M. L. Foo, J. W. Lynn, H. W. Zandbergen, G. Lawes, Y. Wang, B. H. Toby, A. P. Ramirez, N. P. Ong, and R. J. Cava, *J. Phys.: Condens. Matter* **16**, 5803 (2004).
- ⁵⁹ F.-T. Huang, G. J. Shu, M.-W. Chu, Y. K. Kuo, W. L. Lee, H. S. Sheu, and F. C. Chou, *Phys. Rev. B* **80**, 144113 (2009).
- ⁶⁰ J. Wen, A. Rüegg, C.-C. J. Wang, and G. A. Fiete, arXiv:1005.4061 (2010).
- ⁶¹ A. Lichtenstein, M. Katsnelson, and G. Kotliar, in *Electron Correlations and Materials Properties 2* (Kluwer Academic, 2003).
- ⁶² G. Biroli, O. Parcollet, and G. Kotliar, *Phys. Rev. B* **69**, 205108 (2004).
- ⁶³ T. Maier, M. Jarrell, T. Pruschke, and M. H. Hettler, *Rev. Mod. Phys.* **77**, 1027 (2005).
- ⁶⁴ M. Ferrero, P. S. Cornaglia, L. D. Leo, O. Parcollet, G. Kotliar, and A. Georges, *Europhys. Lett.* **85**, 57009 (2009).
- ⁶⁵ M. Capone, L. Capriotti, F. Becca, and S. Caprara, *Phys. Rev. B* **63**, 085104 (2001).
- ⁶⁶ B. Kyung, *Phys. Rev. B* **75**, 033102 (2007).
- ⁶⁷ I. R. Mukhamedshin, H. Alloul, G. Collin, and N. Blanchard, *Phys. Rev. Lett.* **93**, 167601 (2004).
- ⁶⁸ H. Sakurai, N. Tsujii, and E. Takayama-Muromachi, *Physica B* **378** (2006).
- ⁶⁹ L. Balicas, Y. J. Jo, G. J. Shu, F. C. Chou, and P. A. Lee, *Phys. Rev. Lett.* **100**, 126405 (2008).
- ⁷⁰ A. Zorkovská, A. Baran, M. Kajaková, A. Feher, J. Sebek, E. Santavá, C. T. Lin, and J. B. Peng, *Phys. Stat. Sol. (b)* **247**, 665 (2010).
- ⁷¹ M. Lee, L. Viciu, L. Li, Y. Wang, M. L. Foo, S. Watauchi, R. A. Pascal, R. J. Cava, and N. P. Ong, *Nat. Mat.* **5**, 537 (2006).
- ⁷² O. I. Motrunich and P. A. Lee, *Phys. Rev. B* **69**, 214516 (2004).
- ⁷³ S. R. Hassan, L. de Medici, and A.-M. S. Tremblay, *Phys. Rev. B* **76**, 144420 (2007).
- ⁷⁴ M. Bejas, A. Greco, A. Muramatsu, and A. Foussats, *Phys. Rev. B* **77**, 075131 (2008).
- ⁷⁵ D. Qian, D. Hsieh, L. Wray, Y.-D. Chuang, A. Fedorov, D. Wu, J. L. Lue, N. L. Wang, L. Viciu, R. J. Cava, et al., *Phys. Rev. Lett.* **96**, 216405 (2006).
- ⁷⁶ V. Brouet, A. Nicolaou, M. Zacchigna, A. Tejada, L. Patthey, S. Hébert, W. Kobayashi, H. Muguerra, and D. Grebille, *Phys. Rev. B* **76**, 100403 (2007).
- ⁷⁷ A. Nicolaou, V. Brouet, M. Zacchigna, I. Vobornik, A. Tejada, A. Taleb-Ibrahimi, P. L. Fèvre, F. Bertran, S. Hébert, H. Muguerra, et al., *Phys. Rev. Lett.* **104**, 056403 (2010).
- ⁷⁸ J. Bobroff, S. Hébert, G. Lang, P. Mendels, D. Pelloquin, and A. Maignan, *Phys. Rev. B* **76**, 100407 (2007).
- ⁷⁹ Y. Nagaoka, *Phys. Rev.* **147**, 392 (1966).
- ⁸⁰ J. Kanamori, *Progr. Theor. Phys.* **30**, 275 (1963).
- ⁸¹ H. Tasaki, *J. Phys.: Condens. Matter* **10**, 4353 (1998).
- ⁸² K. Penc, H. Shiba, F. Mila, and T. Tsukagoshi, *Phys. Rev. B* **54**, 4056 (1996).
- ⁸³ J. Merino, R. H. McKenzie, and B. J. Powell, *Phys. Rev. B* **80**, 045116 (2009).
- ⁸⁴ There are some minor differences in the free-energy plot of Fig. 19 compared to the one presented in Ref. 49. This is due to the fact that here a smaller gaussian smearing was used in the k-point integration and that technical difficulties in the phase stabilization for $x > 0.9$ were solved by improved mixing procedures for the solution of the saddle-point equations.